Monthly Notices
of the
ROYAL ASTRONOMICAL SOCIETY

MNRAS **434,** 3454–3462 (2013)
Advance Access publication 2013 July 26

doi:10.1093/mnras/stt1257

Jets and the accretion flow in low-luminosity black holes

Emma Gardner★ and Chris Done

Department of Physics, University of Durham, South Road, Durham DH1 3LE, UK

Accepted 2013 July 9. Received 2013 July 8; in original form 2012 July 30

ABSTRACT

The X-ray spectra of black hole binaries (BHB) in the low/hard state (LHS) first harden as the flux decreases, then soften. This change in behaviour has been variously attributed to either the X-rays switching from being produced in the flow to being dominated by the jet, or to the flow switching seed photons from the disc to self-generated seed photons from cyclo-synchrotron. Here, we build a simple truncated disc, hot inner flow, plus standard conical synchrotron jet model to explore what this predicts for the X-ray emission mechanism as a function of mass accretion rate.

We find that the change in X-ray spectral index can be quantitatively (not just qualitatively) explained by the seed photon switch in the hot flow, i.e. this supports models where the X-rays are always produced by the hot flow. By contrast, standard conical jet models are as radiatively inefficient as the hot flow so there is no transition in X-ray production mechanism with $\dot{m}$. Including the effects of electron cooling allows the jet X-rays to drop more slowly with accretion rate and hence overtake the X-rays from the hot flow; however, this produces a corresponding change in the radio–X-ray correlation, which is not observed. We argue that the unbroken radio–X-ray correlation down to quiescence rules out the jet transition model as an explanation for the trend in X-ray spectral index.

Our favoured model is then a truncated disc with an inner, hot, radiatively inefficient flow which always dominates the hard X-rays, coupled to a conical synchrotron jet which produces the radio emission. However, even this has issues at low $\dot{m}$ as the low optical depth and high temperature of the flow means that the Compton spectrum is not well approximated by a power law. This shows the need for a more sophisticated model for the electron distribution in the hot flow.

Key words: accretion, accretion discs – black hole physics – X-rays: binaries.

1 INTRODUCTION

The low/hard state (LHS) of black hole binaries (BHB) is typically seen at mass accretion rates below a few per cent of the Eddington limit. It is characterized by a hard X-ray spectrum, rising in νf_ν to a peak at a few hundred keV, in sharp contrast to the typical temperature of a few hundred eV expected from an optically thick, geometrically thin accretion disc. These X-rays are also strongly variable on short (sub second) time-scales, again, in sharp contrast to the long (few hour) viscous time-scale expected from even the innermost radii of a thin disc. These properties instead are more typical of the alternative set of solutions of the accretion flow equations, where the flow is geometrically thick and optically thin. The most well known of these alternative solutions are the Advection Dominated Accretion Flow (ADAF) models (Narayan & Yi 1995), but these are only an analytic approximation to what is almost certainly a more complex solution, as the flow must be threaded by magnetic fields. Differential rotation shears the field azimuthally, while buoyancy lifts it vertically, and the combination sets up a turbulent magnetic dynamo which acts to transport angular momentum outwards so material can fall inwards. Close to the horizon, this turbulent field can also produce a jet, as observed in this state (see e.g. the review by Done, Gierliński & Kubota 2007, hereafter DGK07; Fender et al. 2004).

These hot flow solutions are only possible at low mass accretion rates, collapsing to the standard disc solutions when the flow becomes optically thick. This gives a mechanism for the dramatic hard to soft state transition seen in the BHB, and the associated collapse of the radio jet. This transition is complex, but the data can be largely fit into a picture where the thin disc progressively replaces the hot flow down to smaller radii as the mass accretion rate increases. These truncated disc models predict that the contribution from the thin disc becomes stronger with increasing mass accretion rate, increasing the seed photons for Compton cooling of the hot flow, so the hard X-ray spectrum becomes softer, as observed. All

★E-mail: e.l.gardner@dur.ac.uk

time-scales associated with the disc truncation radius will decrease, giving a qualitative (and now quantitative) framework in which to explain the correlated increase in characteristic frequencies of the time variability (DGK07, Ingram, Done & Fragile 2009; Ingram & Done 2011, 2012).

While this is an attractive picture, it is still somewhat controversial. The LHS sometimes shows a soft component whose temperature and luminosity imply a very small emitting area, not consistent with the large radius expected for a truncated disc (Rykoff et al. 2007; Reis, Fabian & Miller 2010). While some of this can be explained by continuum modelling, irradiation and assumptions about the inner disc boundary condition (e.g. Gierliński, Done & Page 2008; Makishima et al. 2008), there is still an issue for the lowest mass accretion rate spectra (Reis, Miller & Fabian 2009). However, this can still be consistent with the truncated disc picture if this component is instead produced by clumps torn from the edge of the disc in the truncation process (Chiang et al. 2010), which might also explain the variability seen in this component (Uttley et al. 2011). The radii derived from the iron line profile are even more controversial, but issues with instrumental effects and continuum modelling again mean that this is not definitive evidence ruling out a truncated disc for the LHS (cf. Miller et al. 2006; Done & Diaz Trigo 2010; Reis et al. 2010; Kolehmainen, Done & Díaz Trigo 2011). Thus, we assume a truncated disc geometry in this paper, and quantitatively explore its consequences for the emission spectra of BHB.

In particular, the data show that the X-ray spectral index first becomes harder, but then softens again below a (Eddington-scaled) luminosity of $L/L_{\rm Edd} \sim 10^{-2}$ (e.g. Corbel, Koerding & Kaaret 2008; Russell et al. 2010; Sobolewska et al. 2011, hereafter S11). The truncated disc/hot inner flow model gives a possible explanation for this behaviour of the X-ray spectral index. The disc recedes as mass accretion rate drops, which leads to a decrease in the seed photon luminosity intercepted by the hot flow so its Compton spectrum hardens. However, there is another source of seed photons, from cyclo-synchrotron emission generated within the flow itself by the hot electrons spiralling in the turbulent magnetic field. This source of seed photons increases as the mass accretion rate drops, as the drop in density means that the emission is much less self-absorbed and this more than compensates for the drop in emissivity. Thus, the flow should make a transition from hardening due to Compton scattering on the receding disc, to softening due to Compton scattering of cyclo-synchrotron photons within the flow (S11).

While this works qualitatively, S11 did not test whether this could work quantitatively. Here, we build a simple truncated disc/hot inner flow model and explore whether this can indeed match the observed X-ray spectral index behaviour. Such models have been built before but these often focus on the ADAF, so neglect seed photons from an outer truncated disc (Merloni, Heinz & di Matteo 2003; Yuan, Cui & Narayan 2005; Yuan et al. 2007; Qiao & Liu 2013). The ones which do include seed photons from the disc use such a large disc truncation radius (10^4 Schwarzschild radii) that these have negligible effect (Esin, McClintock & Narayan 1997; Narayan, Barret & McClintock 1997).

We also explore the alternative possibility for the change in X-ray spectral index, where this marks instead the change from a flow-dominated to a jet-dominated X-ray spectrum (Russell et al. 2010; S11). Such a transition to a jet-dominated flow (JDAF) was predicted by Yuan & Cui (2005) and there are coupled ADAF-jet models in the literature, where the X-rays are produced by synchrotron jet emission at low mass accretion rates (e.g. Yuan & Cui 2005; Yu, Yuan & Ho 2011).

Yet another approach to explain the LHS uses JDAF models at all $\dot{m}$, so that the X-rays are always dominated by the jet (e.g. Falcke, Körding & Markoff 2004). However, more recent JDAF models now also include some (often dominant) contribution to the hard X-ray spectrum from Comptonization in a hot flow (Markoff, Nowak & Wilms 2005; Nowak et al. 2011). The focus in these papers has been to (successfully) fit the observed SED's, rather than systematically exploring the predicted behaviour of the model as a function of $\dot{m}$ for physically motivated scalings, which is the aim of this work.

Here, we make a simple model of the accretion flow (truncated disc and hot, radiatively inefficient inner flow) to gain a quantitative understanding of how the X-ray spectrum evolves with $\dot{m}$ in terms of the contribution of disc and cyclo-synchrotron seed photons for flow Comptonization. We then couple this to a standard conical jet model (Blandford & Königl 1979; Merloni et al. 2003) to assess the relative contribution of the flow and the jet to the X-ray emission. We use independent constraints on the relative contribution of flow and jet from the observed radio–X-ray correlation (Hannikainen et al. 1998; Corbel et al. 2003; Gallo, Fender & Pooley 2003; with a more recent compilation in Corbel et al. 2013).

We show that a truncated disc and hot inner flow model can quantitatively as well as qualitatively explain the observed change in behaviour of the hard X-ray spectral slope at lower luminosities. By contrast, it is very difficult to make a model in which the X-rays switch from being produced in the flow to being produced in the synchrotron jet. Standard conical jet models are as radiatively inefficient as the hot flow, as both magnetic energy density and relativistic particle pressure scale as $\dot{m}$, so the synchrotron radiation (which is their product) scales as $\dot{m}^2$ (e.g. Merloni et al. 2003; Falcke et al. 2004). Changing the jet scalings to force such a switch produces a clear break in the radio–X-ray correlation (see also Yuan & Cui 2005), which is not observed.

Our favoured model is then a truncated disc with a hot, radiatively inefficient inner flow which always dominates the hard X-rays, coupled to a conical synchrotron jet which produces the radio emission.

However, even this has problems at low $\dot{m}$ as the low optical depth and high temperature of the flow means that the Compton spectrum is not well approximated by a power law, subtly distorting the radio–X-ray correlation from the observed $L_R \propto L_X^{0.7}$ relation. This shows the need for a more sophisticated accretion flow model, perhaps including non-thermal electrons (Malzac & Belmont 2009; Vurm & Poutanen 2009), and/or an inhomogeneous flow (Veledina, Poutanen & Vurm 2012).

2 THE FIDUCIAL TRUNCATED DISC/HOT INNER FLOW MODEL

In all the following, we use dimensionless radii $r = R/R_g$ where $R_g = GM/c^2$, and mass accretion rates $\dot{m} = \dot{M}/\dot{M}_{\rm Edd}$, where the Eddington limit $L_{\rm Edd} = \eta \dot{M}_{\rm Edd} c^2$ and $\eta = 0.057$ for a Schwarzschild black hole with innermost stable circular orbit $r_{\rm isco} = 6$. We plot models for a $10\,{\rm M}_\odot$ black hole.

Our main aim is to explore the origin of the X-ray flux in the LHS, first whether the truncated disc/hot inner flow model can produce the observed change in behaviour of spectral index with $\dot{m}$, and then to see whether this can also be produced by jet models. Previous models which included both truncated disc seed photons and internally generated cyclo-synchrotron seed photons (Esin et al. 1997; Narayan et al. 1997) did not explicitly explore this, and are also based on a pure ADAF model for the accretion flow. Such pure ADAF models are too hot and optically thin (maximum optical depth $\tau \propto \dot{m} < 1$) to match the observed hard X-ray emission (Yuan

& Zdziarski 2004). Allowing advection to be negative (heating the flow) as well as positive (assumed in the ADAF solution) takes the (luminous hot accretion flow: LHAF) models closer to the data, but there is still a clear mismatch, with data extending up to an optical depth of $\tau \sim 2$ (Yuan & Zdziarski 2004). This probably reflects the fact that all such analytic models are only an approximation to a more complex reality, with magnetic fields threading the flow. Hence, rather than build a full ADAF/LHAF model, which is known to not match the data, we instead take the key aspects of these models (radiatively inefficient flow, i.e. luminosity $L \propto \dot{m}^2$, which exists only up to a maximum mass accretion rate, $\dot{m}_c$) and set the parameters of this flow from the data, i.e. we take $\dot{m}_c = 0.1$ and $\tau = \tau_{\rm max}(\dot{m}/\dot{m}_c)$ with $\tau_{\rm max} = 2$ (e.g. Ibragimov et al. 2005; Torii et al. 2011; Yamada et al. 2013).

In the truncated disc/hot inner flow geometry, this radiatively inefficient flow exists inside a Shakura–Sunyaev disc truncated at radius $r_t \geq r_{\rm isco}$. Evaporation of the cool disc by thermal conduction from a hot corona is known to produce this geometry at low mass accretion rates (Meyer & Meyer-Hofmeister 1994; Liu et al.1999; Liu et al. 2002; Mayer & Pringle 2007), where it typically gives $r_t \propto \dot{m}^{-1/2}$ below the critical mass accretion rate, $\dot{m}_c$, at which the hot flow collapses (e.g. Czerny, Rózańska & Kuraszkiewicz 2004). Evaporation models show that the disc is still substantially truncated at this critical mass accretion rate, but the value of this minimum truncation radius is $\sim 40\,R_g$ ($20R_{\rm sch}$: Czerny et al. 2004). However, the evaporation rates assume the hot flow is an ADAF, whereas our flow is denser and cooler. The conductive flux depends more strongly on density, so we expect stronger evaporation. This combined with weaker constraints on the observed disc radius in the LHS (Yamada et al. 2013) motivates us to choose $r_t = 20(\dot{m}/\dot{m}_c)^{-1/2}$.

We assume a standard Novikov–Thorne emissivity for a disc from $r_{\rm out} = 10^5$ to r_t, and assume that all this energy thermalizes, giving $L_{\rm disc}$. The remaining energy from the Novikov–Thorne emissivity from r_t to $r_{\rm isco}$ is available to power the hot flow, $L_{\rm hot,\,power}$, but this is radiatively inefficient so we take the actual radiated power to be $L_{\rm hot} = (\dot{m}/\dot{m}_c)L_{\rm hot,power}$, i.e. assume that the flow is as efficient as a thin disc at $\dot{m}_c$.

The hot flow radiates $L_{\rm hot}$ via Comptonization (which depends on seed photon luminosity from both the disc and cyclo-synchrotron photons generated by the electrons interacting with the magnetic field in the hot flow) and bremsstrahlung (which depends on density). We assume that the hot flow is a homogeneous sphere. The obvious radius of this sphere is r_t, but the emission should be centrally concentrated, so instead we assume that all the energy is dissipated in a region $r_h = 20$. At any radius r in the disc, we calculate the fraction of photons illuminating the hot flow, so the seed photon luminosity, $L_{\rm seed,\,disc}$ is given by this integrated over all the disc from $r_{\rm out}$ to r_t. The density of the flow is then $n \sim \tau/(\sigma_T r_h R_g)$.

Radiatively inefficient flows are also generically two temperatures, with ion temperature set by the virial temperature $kT_{\rm ion} \approx m_p c^2/r$, while the electron temperature is set by the balance of heating and cooling. We assume that the flow is homogeneous within r_h so $kT_{\rm ion} \sim m_p c^2/r_h$. Simulations show that the energy density in the tangled magnetic field saturates to $\sim$10 per cent of the gas pressure, so $U_B = B^2/(8\pi) = 0.1nkT_{\rm ion}$. The cyclo-synchrotron emission from the hot flow then extends as an approximate steep power law from $\upsilon_B = eB/(2\pi m_e c) = 2.6 \times 10^6 B$. However, the majority of this emission is self-absorbed, so the emission peaks instead at the self-absorption frequency $\nu_{\rm csa} = \frac{3}{2}\nu_B \theta_e^2 x_m$, where the electron temperature $\theta_e = kT_e/m_e c^2$ (found iteratively, see below) and x_m typically has values of a few hundred to a few thousand (see Appendix for full details). The luminosity is then $L_{\rm seed,cyclo} \propto n\nu_{\rm csa}^2 V$, where $V = \frac{4}{3}\pi r_h^3 R_g^3$ is the volume of the hot flow.

The total seed photon luminosity $L_{\rm seed} = L_{\rm seed,\,disc} + L_{\rm seed,\,cyclo}$. We take the seed photon energy ($\nu_{\rm seed}$) as the weighted mean of the inner disc temperature and the cyclo-synchrotron self-absorption frequency, as defined in equation A11 in the Appendix. The electron temperature can then be derived self-consistently from balancing heating ($L_{\rm hot}$) and cooling (determined by $L_{\rm seed}$, but also including bremsstrahlung) rates using the publicly available EQPAIR code. This calculates the electron temperature and resulting emission spectrum from a homogeneous sphere, given inputs of the heating power to the electrons ($L_{\rm hot}$), the optical depth and size of the region (τ and r_h) and the power and typical energy of the seed photons ($L_{\rm seed}$ and $\nu_{\rm seed}$) for Compton cooling (Coppi 1999). The resulting spectrum incorporates both bremsstrahlung and Compton components and does not assume that the Compton emission can be approximated as a power law. This is increasingly important as the flow density drops, as each successive Compton order scattering is separated by a factor of $1/\tau$, making the spectrum increasingly bumpy as the mass accretion rate decreases.

To summarize: our accretion flow model consists of a truncated disc where the truncation radius increases with decreasing $\dot{m}$, and a radiatively inefficient inner hot flow powered by the remaining gravitational energy that is not dissipated in the truncated disc. We allow the optical depth of this hot flow to decrease with $\dot{m}$, and use both the external disc photons intercepting the hot flow and internal cyclo-synchrotron photons generated within the hot flow as seed photons for Comptonization.

2.1 Spectral changes with accretion rate

Fig. 1 shows a sequence of model spectra for $\dot{m} = \dot{m}_c = 10^{-1}$ to $\dot{m} = 4 \times 10^{-3}$ (i.e. $r_t = 20$ to 100). Solid lines show the total

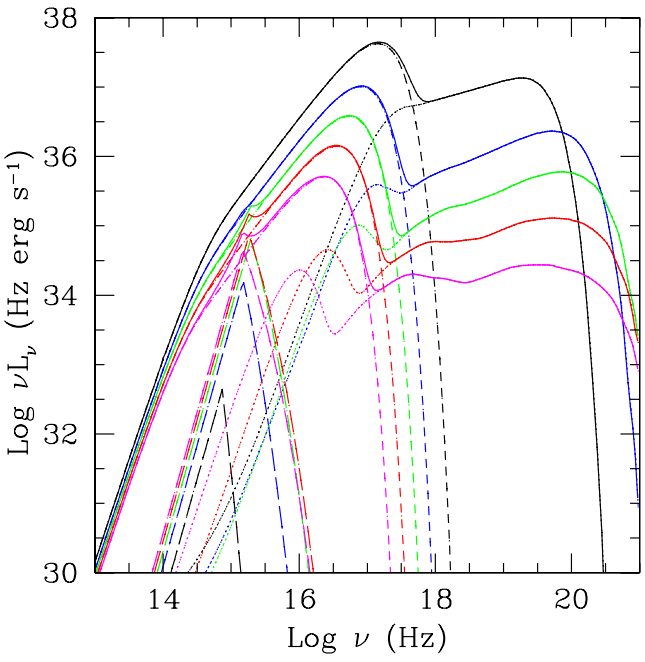

Figure 1. Model SEDs, with truncated disc (short dashed line), hot flow cyclo-synchrotron emission (long dashed line) and Comptonization of both disc and cyclo-synchrotron seed photons (dotted line) for increasing truncation radius: 20 (black), 35 (blue), 50 (green), 70 (red) and 100 R_g (magenta). Solid line shows sum of all three components.

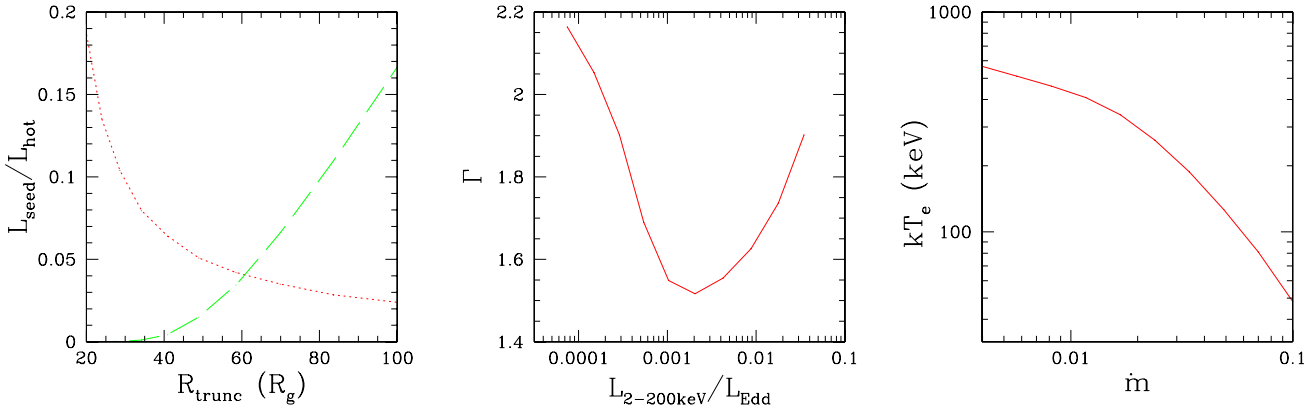

Figure 2. (a) Seed photon luminosity as a function of truncation radius, for disc seed photons (red dotted line) and cyclo-synchrotron seed photons (green dashed line). For $R_{\rm trunc} \gtrsim 60\,R_g$ ($\dot{m} \lesssim 0.01$) the dominant source of seed photons is cyclo-synchrotron emission from the hot flow. (b) Photon index as a function of 2–200 keV X-ray luminosity, showing softening of the X-ray spectrum at low luminosities as cyclo-synchrotron seed photons begin to dominate. (c) Hot flow electron temperature as a function of mass accretion rate, where $\dot{m} = \dot{M}/\dot{M}_E$.

emission, long dashed, short dashed and dotted lines show the individual components of cyclo-synchrotron, truncated disc and Comptonization, respectively.

The proportion of luminosity in the disc compared to the hot flow, $L_{\rm disc}/L_{\rm hot} \approx (\dot{m}/\dot{m}_c)^{-1}(\frac{r_t}{r_{\rm isco}} - 1)^{-1}$. Since we also know how r_t depends on $\dot{m}$ we can simplify this further to $\approx 0.3(\dot{m}/\dot{m}_c)^{-1/2} \propto r_t$. Thus, decreasing $\dot{m}$ by a factor of 25 increases the disc truncation radius by a factor of 5 and increases $L_{\rm disc}/L_{\rm hot}$ by a factor of 5. This is not a large factor, but is evident in Fig. 1 by comparing the ratio between the peak νf_ν flux of the disc and Comptonized emission for the highest and lowest $\dot{m}$ spectra.

However, the ratio between $L_{\rm seed,\,disc}/L_{\rm hot}$ changes by much more than $L_{\rm disc}/L_{\rm hot}$ as the fraction of seed photons intercepted by the hot flow drops as r_t increases. The seed photons from the disc which illuminate the hot flow are integrated over the entire disc, but both the disc luminosity and the fraction which are intercepted by the flow will peak at r_t. Hence $L_{\rm seed,disc} \approx L_{\rm disc}(r_h/r_t)\arcsin(r_h/r_t) \approx \frac{\dot{m}}{r_t}(r_h/r_t)^2 \propto \dot{r_t}^{-5} \propto \dot{m}^{2.5}$. Thus, $L_{\rm seed,disc}/L_{\rm hot} \propto \dot{m}^{2.5}/\dot{m}^2 \propto \dot{m}^{1/2} \propto r_t^{-1}$. Thus, while $L_{\rm disc}/L_{\rm hot}$ increases by a factor of 5 as $\dot{m}$ decreases, $L_{\rm seed,\,disc}/L_{\rm hot}$ decreases by a factor of 5 (see red line in Fig. 2a). If this were the only source of seed photons, the spectrum should harden substantially. However, there are also seed photons from the cyclo-synchrotron emission. These have $L_{\rm seed,cyc} \propto n\nu_{\rm csa}^2 \propto n(B\theta_e^2)^2 \propto \dot{m}^2\theta_e^4$, so $L_{\rm seed,cyc}/L_{\rm hot} \propto \theta_e^4$. This increases as $\dot{m}$ decreases, as θ_e increases as accretion rate drops (see below). The green line in Fig. 2(a) shows that the internally generated cyclo-synchrotron emission starts to dominate over seed photons from the disc at $r_t > 60$ (equivalently $\dot{m} \leq 10^{-2}$). Thus, the total $L_{\rm seed}/L_{\rm hot}$ reaches a minimum at this point, and then starts to increase. This change in dominant seed photons can also be seen in Fig. 1 as the Compton spectrum extends to lower energies reflecting the lower seed photon energy of the cyclo-synchrotron photons.

The Comptonization spectral slope is set by $L_{\rm seed}/L_{\rm hot}$, so this also shows a minimum corresponding to the minimum $L_{\rm seed}/L_{\rm hot}$. Fig. 2(b) shows the resulting 2–10 keV power-law index and 2–200 keV bolometric luminosity, L_{2-200}. Our minimum in photon index occurs at 2–3 $\times\ 10^{-3}L_{\rm Edd}$, a factor of 2–3 below that shown by the data in S11. Given the simple assumptions made about the structure of the flow, this is probably not significant. In particular, changing the efficiency of the hot flow from a simple $\propto \dot{m}$ to the more complex behaviour calculated by Xie & Yuan (2012) specifically for an ADAF model would make this discrepancy smaller. Thus, the model is able to quantitatively describe a key observation of the LHS, namely that the X-ray spectrum hardens with decreasing $\dot{m}$ and then softens again by the change in seed photons from the disc to internally generated cyclo-synchrotron. This softening of the Comptonized emission can be seen by eye in the spectra of Fig. 1 by comparing the slope of the tail at the highest and lowest luminosity.

Qiao & Liu (2013) find a similar trend in photon index using a full ADAF calculation. However, their disc-corona geometry is rather different from that considered here. They focus on the residual inner disc which can remain after considering thermal conduction from the hot flow (Liu, Meyer & Meyer-Hofmeister 2006; Liu, Done & Taam 2011). At the highest mass accretion rates, the disc extends all the way down to the innermost stable circular orbit. Then, as accretion rate drops a gap opens up between the inner and outer disc at $\sim 200\,R_g$, and this gap extends inwards and outwards as $\dot{m}$ decreases until the entire inner disc evaporates. Thus, their drop in seed photons comes from a decreasing outer extent of the inner disc, whereas in our model it comes from the increasing inner radius of the outer disc. Nonetheless, both models have a drop in seed photons with mass accretion rate, so the spectra harden, and then both models show the characteristic minimum as self-generated cyclo-synchrotron photons take over as the dominant seed photons in the hot flow.

Fig. 2(c) shows the resulting electron temperature, set from the balance of heating and cooling. The heating rate is $\propto \dot{m}^2$, and cooling is predominantly Compton cooling so is $\propto 4\theta_e\tau L_{\rm seed}$. At high $\dot{m}$, the seed photons are from the disc so the cooling rate is $\propto 4\theta_e\tau\frac{\dot{m}}{r_t}(\frac{r_h}{r_t})^2$. Hence $\theta \propto \dot{m}^{-3/2}$, quite close to the observed dependence. Conversely, when seed photons from cyclo-synchrotron cooling dominate, the Compton cooling rate is $\propto 4\theta_e\tau n\nu_{\rm csa}^2$, where $\nu_{\rm csa} \propto B\theta_e^2$ so $\theta_e \propto \dot{m}^{-0.2}$. The strong increase in seed photons with increasing temperature leads to increasing cooling with decreasing mass accretion rate, which counteracts much of the decrease in cooling from the decrease in optical depth. Thus, the electron temperature increases much more slowly as the mass accretion rate decreases. Again this can be seen in the spectra of Fig. 1, where the electron temperature (marked by the high energy rollover of the tail) first increases markedly with decreasing mass accretion rate, then stabilizes. This changing temperature dependence on accretion rate is a testable prediction of the model. Current observations already

show that the behaviour in the brightest LHSs do indeed show the predicted decrease in temperature with increasing $\dot{m}$ (Motta, Belloni & Homan 2009; Torii et al. 2011), but future observations with the more sensitive Soft Gamma-ray Detector (60–600 keV bandpass) on ASTRO-H (Takahashi et al. 2012) will be able to constrain the temperature down to much lower $\dot{m}$.

The other obvious change in the Comptonized emission is that it is progressively less well described by a power law as $\dot{m}$ decreases and $\tau \ll 1$. At such low optical depths, the individual scattering orders become visible, giving a more complex spectral shape. Data are rarely fitted with such low optical depths, as X-ray observations do not show the strong first Compton peak, which would be clearly visible in the X-ray regime if the seed photons were provided by a disc. From our model it is clear that the dominant source of seed photons at these mass accretion rates is cyclo-synchrotron emission. This brings the first peak out of the X-ray regime, leaving the X-ray spectrum to be dominated by higher order scattering with less extreme curvature. Nevertheless, this is still not visible in X-ray spectra from low $L/L_{\rm Edd}$ flows (e.g. Corbel et al. 2006). We suggest the reason for this is that our model assumes that the electrons in the hot flow completely thermalize. An initially non-thermal acceleration process will probably thermalize via self-absorption of its own cyclo-synchrotron radiation in bright LHSs (Malzac & Belmont 2009; Poutanen & Vurm 2009). However, the thermalization time-scale increases as the source luminosity drops, so the electron distribution retains more of its initially non-thermal character, giving a non-thermal power-law Compton spectrum (e.g. Veledina, Vurm & Poutanen 2011).

3 FIDUCIAL CONICAL JET

The radio jet is an important part of the energy budget of the black hole accretion flow, with kinetic energy comparable to the hard X-ray luminosity at $\dot{m}_c$ (e.g. Cyg X-1: Gallo et al. 2005; Russell et al. 2007; Malzac, Belmont & Fabian 2009). Hence, we take the jet $L_{KE,\rm max} = \dot{m}_c L_{\rm Edd} = 1.3 \times 10^{38}$ ergs s^{-1}.

We add a standard conical jet model on to our accretion flow (e.g. Blandford & Königl 1979; hereafter BK79; Merloni et al. 2003; Falcke et al. 2004), assuming that some acceleration process operates continuously down the jet, so that a small fraction of the electrons in the jet form a relativistic particle distribution. The electrons radiate via synchrotron to produce a broad-band spectrum from radio to X-rays. If these radiative losses are high then this will affect the self-similar jet structure. Hence, we limit the radiative luminosity to 10 per cent of the kinetic luminosity of the jet, i.e. we make a maximally radiatively efficient, self-similar jet.

Parameters for a standard conical jet include the distance from the black hole at which the material is accelerated, Z_0 (the jet base). We make the standard assumption that the energy is transported by Poynting flux from r_h in the hot flow, where the jet is presumably launched, to z_0 without any radiative losses. The self-similar behaviour then extends out from Z_0 to a distance of $Z_{\rm max} = 10^6 Z_0$, where $Z = zR_g$ is distance along the jet. Distance perpendicular to the jet is $R_j = \rho R_g = \phi Z$, where ϕ is constant for a conical jet.

We use observations to set the bulk Lorentz factor $\Gamma = 1.2$ and opening angle $\phi = 0.1$ (e.g. Gallo et al. 2005). We assume that these stay constant with $\dot{m}$. We transform all specific luminosities L_ν from jet frame to observer frame by multiplying by $\delta^3 = (\Gamma - \sqrt{\Gamma^2 - 1}\cos\psi)^{-1}$, assuming a mean inclination angle $\psi = 60^\circ$ and boost all frequencies by δ.

In such a geometry, the magnetic field energy density $U_B(z) \propto z^{-2}$ (BK79). Turbulence in the field probably results in scaling between the relativistic particle and magnetic pressures, so $U_{\rm rel}(z) = m_e c^2 \int_1^{\gamma_{\rm max}} N(z,\gamma)\gamma {\rm d}\gamma = f_{\rm rel} U_B(z)$ where $N(z,\gamma)$ is the electron distribution at each point z of the jet. We make the standard assumptions that $N(z,\gamma) = K(z)\gamma^{-p}$ with $p = 2.4$ between $\gamma_{\rm min} = 1$ and $\gamma_{\rm max} = 10^5$. Hence the optically thin synchrotron emission has energy index $\alpha = (p-1)/2 = 0.7$, i.e. it rises in νf_ν with energy output peaking at the highest frequency $\nu_{\rm max} = 4/3\gamma_{\rm max}^2 \nu_B$.

The power-law synchrotron emission becomes optically thick to self-absorption below $\nu_{\rm ssa} \propto K^{2/7} B^{5/7} R_j^{2/7} \propto (z/z_0)^{-1}$ (Ghisellini, Maraschi & Treves 1985), i.e. decreases with larger distance along the jet. The flux at this point, $L(\nu_{\rm ssa})_{\rm sync} \propto (z/z_0)^{-1}(\nu_{\rm ssa}/\nu_B)^{-(p-1)/2}{\rm d}Z \propto (z/z_0)^{-1}{\rm d}Z \propto {\rm d}\log Z$. Thus, the self-absorbed spectra from each part of the jet sum together to produce the characteristic 'flat spectrum' (i.e. energy index $\alpha = 0$: BK79) at low frequencies.

We do not include the self-consistent inverse Compton emission from the jet, since this contributes only at higher energies (e.g. Zdziarski, Lubiński & Sikora 2012) and the baseline model we are testing is one where the X-rays are produced by synchrotron from the jet.

3.1 Jet at $\dot{m}_c$

We anchor the jet at $\dot{m}_c = 0.1$ using observational constraints. The observed break from optically thick to optically thin synchrotron in a bright LHS from GX 339−4 is $\nu_{\rm ssa,0} \sim 10^{13.5}$, and the 10 GHz radio luminosity from the sum of self-absorbed jet components is six orders of magnitude below the X-ray emission (Gandhi et al. 2011), i.e. $\nu L_\nu \sim 10^{31}$ ergs s^{-1} at 10 GHz. This sets $B(z_0) \sim 3.5 \times 10^4$ G (i.e. $K(z_0) = 2.4 \times 10^{12}$ cm^{-3} for $f_{\rm rel} = 0.1$) and $z_0 \sim 5300$. This gives a total radiated luminosity of 10 per cent of the kinetic jet power, as described above for a maximal radiatively efficient jet.

We note that in these standard conical jets the fraction of radiative power to kinetic power is not constant down the jet, as the radiation depends on both magnetic and electron energy density so is $\propto (z/z_0)^{-4}{\rm d}V$ while the jet kinetic energy is simply $\propto (z/z_0)^{-2}{\rm d}V$.

3.2 Jet scaling with mass accretion rate – transition to a jet-dominated state

We then assume that the jet kinetic power $\propto \dot{m}$, and that all energy densities scale as $\dot{m}/\dot{m}_c$ (Heinz & Sunyaev 2003) so that $B(z,\dot{m}) = B_0(z_0,\dot{m}_c)(z/z_0)^{-1}(\dot{m}/\dot{m}_c)^{1/2}$ and $K(z,\dot{m}) = K_0(z_0,\dot{m}_c)(z/z_0)^{-2}(\dot{m}/\dot{m}_c)$. Fig. 3(a) shows a sequence of spectra for decreasing $\dot{m}$ using this coupled accretion flow–jet model. Our model reproduces the $L_R \propto L_X^{0.7}$ radio–X-ray correlation, as shown in Fig. 3(b). The X-rays come from a radiatively inefficient accretion flow and are therefore proportional to $\dot{m}^2$. The radio is from the optically thick jet, where it has a flat spectrum so $L_R \propto B_0^{1.2} K_0^{0.8} \propto \dot{m}^{1.4}$ for any model where the magnetic and relativistic particle energy densities scale with $\dot{m}$, hence $L_R \propto L_X^{0.7}$ for a radiatively inefficient X-ray flow (e.g. Heinz & Sunyaev 2003; Merloni et al. 2003). The model slightly deviates from this relation at low $\dot{m}$, because of the spectral curvature in our model at low $\dot{m}$ which changes the scaling over a small bandpass ($L_{3-9\,\rm kev}$). The dashed line in Fig. 3(b) shows that a wider bandpass recovers the relation even down to the lowest luminosities. As discussed in Section 2.1, this detailed issue can probably be circumvented by a proper treatment of the self-consistent electron distribution in the hot flow (as in Veledina et al. 2011).

The jet emission does not ever dominate the total hard X-ray emission, but remains an approximately constant factor below the

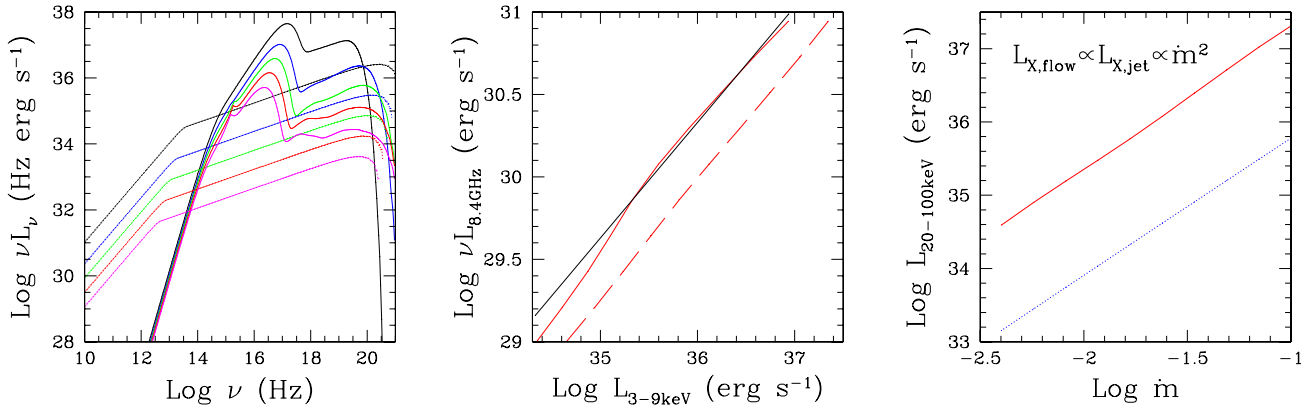

Figure 3. (a) Model SEDs, including synchrotron jet emission (dotted line) for increasing truncation radius: 20 (black), 35 (blue), 50 (green), 70 (red) and 100 R_g (magenta). (b) $L_R \propto L_X^{0.7}$ radio–X-ray correlation (black line), together with correlation from coupled accretion flow/jet model (solid red line). The dashed red line shows radio–X-ray correlation using $L_{20-100\,\mathrm{keV}}$ X-ray luminosity instead of $L_{3-9\,\mathrm{keV}}$. (c) X-ray luminosity as a function of mass accretion rate, where $\dot{m} = \dot{M}/\dot{M}_E$, for X-rays from the radiatively inefficient accretion flow (solid red line) and X-rays from the jet (dotted blue line).

hot flow (Fig. 3c). This is because the optically thin synchrotron luminosity $L_{X,\mathrm{jet}} \propto K_0 U_{B,0} \propto \dot{m}^2$ so it also follows a radiatively inefficient scaling. This is in contrast to the jet *kinetic* luminosity, which does scale as $\dot{m}$. Thus, while the *kinetic* luminosity of the jet can easily dominate the radiative energy of the flow, the *radiated* energy of the jet drops as fast as that from the flow. Thus, there is no transition in the X-ray spectrum from being dominated by the radiatively inefficient hot flow to being dominated by the synchrotron emission of a conical, self-similar jet (see also Merloni et al. 2003; Falcke et al. 2004). There are instances in the literature where there is a flow–jet transition in the X-ray flux, but these use models where the flow is radiatively efficient (no advection: Fender, Gallo & Jonker 2003) and/or have a jet kinetic power which does not scale as $\dot{m}$ (Yuan & Cui 2005).

3.3 Jet scaling with electron cooling

The discussion above assumes that the energy density in relativistic particles scales as the energy density in the jet, i.e. $\int N(\gamma)\gamma \mathrm{d}\gamma \propto \dot{m}/M$ (Heinz & Sunyaev 2003). However, a better approach is to say that it is the injected electron distribution, $Q(\gamma) = Q_0 q(\gamma)$, which scales, and then cools into a steady-state distribution $N(\gamma) = Kn(\gamma)$ (e.g. for Blazar jets: Ghisellini et al. 2010). In this case, the injected distribution is normalized to the available power (i.e. $Q_0 \propto \dot{m}$), so that K now scales as $K \propto Q_0/U_{\mathrm{seed}}$. For synchrotron cooling, $U_{\mathrm{seed}} = U_B \propto \dot{m}$ giving K constant with accretion rate. Hence $L_{X,\mathrm{jet}} \propto K_0 U_{B,0} \propto \dot{m}$, such that it is possible for the jet X-rays to overtake the X-ray luminosity from the flow as accretion rate decreases. However, $L_R \propto B_0^{1.2} K_0^{0.8}$, so the radio luminosity no longer scales as $L_R \propto \dot{m}^{1.4}$ but scales as $L_R \propto \dot{m}^{0.6}$ (Table 1). When the X-rays come from the jet, this gives $L_R \propto L_{X,\mathrm{jet}}^{0.6}$, which is not inconsistent with the data. But for higher accretion rates, when the X-rays come from the flow (and we know $L_{X,\mathrm{flow}}$ must be proportional to $\dot{m}^\beta$ where $\beta > 1$ for a transition to occur at all) this becomes $L_R \propto L_{X,jet}^{0.3}$, which does not match the observed correlation. The optically thick synchrotron from the jet must still drop as $\dot{m}^{1.4}$ to make the $L_X - L_R$ relation when the hot flow dominates.

3.4 Composite jet with electron cooling break

Since energetic electrons cool faster, the electron distribution is expected to be composite, with the electron distribution above some break energy γ_b being dominated by cooling, while below this energy it reflects instead the injected electron distribution (e.g. Markoff et al. 2005; Yuan et al. 2005; Zdziarski et al. 2012). The cooling break energy $\propto 1/(U_B Z) \propto \dot{m}^{-1}$ (Zdziarski et al. 2012, equation 36), so does not depend on mass but increases linearly with decreasing mass accretion rate. For our parameters, the cooling break is $\gamma_{\mathrm{cool}} \sim 1.3$ for $\dot{m} = \dot{m}_c$, increasing to $\gamma_{\mathrm{cool}} \sim 26$ for our lowest $\dot{m}$. Even the highest γ_{cool} is mostly below the synchrotron self-absorption break, so makes very little difference in the spectrum (see e.g. Zdziarski et al. 2012, fig. 5a) or in the predicted X-ray scaling from the completely cooling-dominated jet described above.

3.5 Arbitrary jet scaling

It is possible to contrive situations for a synchrotron jet where the radio scales as $\dot{m}^{1.4}$ but the X-rays scale as $\dot{m}$ (e.g. by allowing z_0 to change with accretion rate). But it is clear that any transition from a flow where $L_X \propto \dot{m}^2$ to this jet, where $L_X \propto \dot{m}$, will

Table 1. Scalings with accretion rate for a standard self-similar conical synchrotron jet, and the same synchrotron jet including cooling. (1) Dependence of radio luminosity on Eddington-scaled accretion rate. (2) Dependence of jet X-ray luminosity on accretion rate. (3) Dependence of flow X-ray luminosity on accretion rate, assuming a radiatively inefficient hot flow. (4) Dominant source of X-ray emission as a function of accretion rate. (5) Index of the radio–X-ray correlation for X-rays from the flow. (6) Index of the radio–X-ray correlation for X-rays from the jet.

Type of jet	L_R	$L_{X,\mathrm{jet}}$	$L_{X,\mathrm{flow}}$	Dominant source of X-ray emission	α_{flow} ($L_R \propto L_{X,\mathrm{flow}}^{\alpha}$)	α_{jet} ($L_R \propto L_{X,\mathrm{jet}}^{\alpha}$)
	(1)	(2)	(3)	(4)	(5)	(6)
Standard	$\dot{m}^{1.4}$	$\dot{m}^2$	$\dot{m}^2$	Either hot flow or jet	0.7	0.7
Cooling	$\dot{m}^{0.6}$	$\dot{m}$	$\dot{m}^2$	Hot flow with a transition to jet X-rays as $\dot{m}$ decreases	0.3	0.6

cause a steepening of the observed $L_R - L_X$ relation (Yuan & Cui 2005). Changing the X-ray behaviour with $\dot{m}$, without a simultaneous change in the behaviour of the optically thick radio emission, necessarily changes the $L_R - L_X$ correlation in a way which is not observed (Corbel et al. 2013). Since we do not observe a change in the radio–X-ray correlation down to quiescence in BHBs (e.g. Corbel et al. 2013 and references therein), we know there can be no transition in dominant X-ray production mechanism down to these luminosities. Whatever dominates the X-rays in the brightest LHS spectra, at the top of the correlation, must dominate at the bottom. This rules out all plausible models in which the X-rays switch from being dominated by the flow to being dominated by the jet.

We note that a break has been observed in the radio–X-ray correlation in active galactic nuclei (AGN) at very low accretion rates ($\dot{m} \sim 10^{-6}$, Yuan, Yu & Ho 2009), but crucially the observed minimum in photon index occurs where the correlation is unbroken, implying that jet emission taking over cannot be the cause.

3.6 Jet-dominated models

Since a switch from flow-dominated to jet-dominated X-ray flux is ruled out by the radio–X-ray correlation, the final possibility is that the X-rays are always dominated by the jet (Falcke et al. 2004). However, our fiducial jet model is already very efficient at producing radiation. To make the jet dominate at $\dot{m}_c$ would require that almost all of the jet kinetic energy was transformed to radiation, which seems unlikely. It would also impact on our assumptions that adiabatic and radiative losses are negligible, and leaves unanswered the question of what causes the change in X-ray behaviour (hardening then softening of the spectral index) as $\dot{m}$ decreases. Jet-dominated models are also unable to fit the high energy rollover seen at high energies seen in the bright LHS ($\dot{m} \sim \dot{m}_c$: Ibragimov et al. 2005; Torii et al. 2011). More spectral and energetic constraints are discussed in Zdziarski et al. (2003) and Malzac et al. (2009).

4 CONCLUSIONS

The observed change in X-ray spectral index as $\dot{m}$ decreases in the LHS (first hardening then softening) can be quantitatively explained by a truncated disc/radiatively inefficient hot inner flow. Seed photons from the disc drop as the disc recedes with decreasing $\dot{m}$ so that self-generated cyclo-synchrotron seed photons in the flow become dominant in Compton cooling. This model can also produce the observed radio–X-ray correlation with the addition of a standard, conical self-similar jet. These standard jets are as radiatively inefficient as the hot flow, so there is no transition from the X-rays being dominated by the flow to being dominated by the jet, which was the alternative explanation for the X-ray spectral behaviour (Russell et al. 2010, S11). Including the effects of cooling allows the jet X-rays to drop more slowly with accretion rate and hence overtake the X-rays from the hot flow; however, such a transition would also necessarily distort the radio–X-ray correlation in a way which is not observed.

Thus, we show that the truncated disc/radiatively inefficient hot flow/standard conical jet model can quantitatively explain the broad-band spectral evolution of BHB in the LHS, with the X-rays always being dominated by the flow, and the radio by the jet. However, at low luminosities, the optical depth in the hot flow is rather small, so the X-ray spectra are no longer a power law and the individual Compton scattering orders can clearly be seen. Yet the observed BHB spectra at these low mass accretion rates (quiescence) are well described by a power law (e.g. Gallo et al. 2006). This discrepancy is even more evident in the low mass accretion rate AGN (e.g. Yu et al. 2011), which has again led to models where the X-rays are dominated by the jet. Since these are inconsistent with the observed radio–X-ray correlation, we suggest instead that this points to a more complex flow, where the electron acceleration process produces an intrinsically non-thermal distribution. Thermalization via cyclo-synchrotron emission and absorption produces the dominant thermal electron population of the bright LHS, while the dramatic increase in seed photons from the disc in the high/soft state means that the power-law distribution is seen (Malzac & Belmont 2009; Vurm & Poutanen 2009). We suggest at very low accretion rates the cooling is so inefficient that thermalization does not happen and the electron distribution remains non-thermal. A non-thermal electron distribution will emit a power-law spectrum, as observed. Hybrid thermal/non-thermal models, especially combined with a multizone approach (Veledina et al. 2012), hold out the possibility to understand the broad-band spectral variability both on long time-scales, with changing accretion rate, and on short time-scales, to understand how fluctuations in the flow can make the observed IR/optical/X-ray correlations (Kanbach et al. 2001; Malzac et al. 2004; Gandhi et al. 2008).

ACKNOWLEDGEMENTS

We acknowledge the referees for useful comments which improved the paper. EG acknowledges funding from the UK STFC.

REFERENCES

Blandford R. D., Königl A., 1979, ApJ, 232, 34 (BK79)
Chiang C. Y., Done C., Still M., Godet O., 2010, MNRAS, 403, 1102
Coppi P. S., 1999, ASP Conf. Ser. Vol. 161, High Energy Processes in Accreting Black Holes. Astron. Soc. Pac., San Francisco, p. 375
Corbel S., Nowak M. A., Fender R. P., Tzioumis A. K., Markoff S., 2003, A&A, 400, 1007
Corbel S., Tomsick J. A., Kaaret P., 2006, ApJ, 636, 971
Corbel S., Koerding E., Kaaret P., 2008, MNRAS, 389, 1697
Corbel S., Coriat M., Brocksopp C., Tzioumis A. K., Fender R. P., Tomsick J. A., Buxton M. M., Bailyn C. D., 2013, MNRAS, 428, 2500
Czerny B., Rózańska A., Kuraszkiewicz J., 2004, A&A, 428, 39
Di Matteo T., Celotti A., Fabian A. C., 1997, MNRAS, 291, 805
Done C., Diaz Trigo M., 2010, MNRAS, 407, 2287
Done C., Gierliński M., Kubota A., 2007, A&AR, 15, 1 (DGK07)
Esin A. A., McClintock J. E., Narayan R., 1997, ApJ, 489, 865
Falcke H., Körding E., Markoff S., 2004, A&A, 414, 895
Fender R. P., Gallo E., Jonker P. G., 2003, MNRAS, 343, L99
Fender R. P., Belloni T. M., Gallo E., 2004, MNRAS, 355, 1105
Gallo E., Fender R. P., Pooley G. G., 2003, MNRAS, 344, 60
Gallo E., Fender R., Kaiser C., Russell D., Morganti R., Oosterloo T., Heinz S., 2005, Nat, 436, 819
Gallo E., Fender R. P., Miller-Jones J. C. A., Merloni A., Jonker P. G., Heinz S., Maccarone T. J., van der Klis M., 2006, MNRAS, 370, 1351
Gandhi P. et al., 2008, MNRAS, 390, L29
Gandhi P. et al., 2011, ApJ, 740, L13
Ghisellini G., Maraschi L., Treves A., 1985, A&A, 146, 204
Ghisellini G., Tavecchio F., Foschini L., Ghirlanda G., Maraschi L., Celotti A., 2010, MNRAS, 402, 497
Gierliński M., Done C., Page K., 2008, MNRAS, 388, 753
Hannikainen D. C., Hunstead R. W., Campbell-Wilson D., Sood R. K., 1998, A&A, 337, 460
Heinz S., Sunyaev R. A., 2003, MNRAS, 343, L59
Ibragimov A., Poutanen J., Gilfanov M., Zdziarski A. A., Shrader C. R., 2005, MNRAS, 362, 1435
Ingram A., Done C., 2011, MNRAS, 415, 2323
Ingram A., Done C., 2012, MNRAS, 419, 2369

Ingram A., Done C., Fragile P. C., 2009, MNRAS, 397, L101
Kanbach G., Straubmeier C., Spruit H. C., Belloni T., 2001, Nat, 414, 180
Kolehmainen M., Done C., Díaz Trigo M., 2011, MNRAS, 416, 311
Liu B. F., Yuan W., Meyer F., Meyer-Hofmeister E., Xie G. Z., 1999, ApJ, 527, L17
Liu B. F., Mineshige S., Meyer F., Meyer-Hofmeister E., Kawaguchi T., 2002, ApJ, 575, 117
Liu B. F., Meyer F., Meyer-Hofmeister E., 2006, A&A, 454, L9
Liu B. F., Done C., Taam R. E., 2011, ApJ, 726, 10
Makishima K. et al., 2008, PASJ, 60, 585
Malzac J., Belloni T., Spruit H. C., Kanbach G., 2004, Nucl. Phys. B, 132, 400
Malzac J., Belmont R., 2009, MNRAS, 392, 570
Malzac J., Belmont R., Fabian A. C., 2009, MNRAS, 400, 1512
Markoff S., Nowak M. A., Wilms J., 2005, ApJ, 635, 1203
Mayer M., Pringle J. E., 2007, MNRAS, 376, 435
Merloni A., Heinz S., di Matteo T., 2003, MNRAS, 345, 1057
Meyer F., Meyer-Hofmeister E., 1994, A&A, 288, 175
Miller J. M., Homan J., Steeghs D., Rupen M., Hunstead R. W., Wijnands R., Charles P. A., Fabian A. C., 2006, ApJ, 653, 525
Motta S., Belloni T., Homan J., 2009, MNRAS, 400, 1603
Narayan R., Yi I., 1995, ApJ, 452, 710
Narayan R., Barret D., McClintock J. E., 1997, ApJ, 482, 448
Nowak M. A. et al., 2011, ApJ, 728, 13
Poutanen J., Vurm I., 2009, ApJ, 690, L97
Qiao E., Liu B. F., 2013, ApJ, 764, 2
Reis R. C., Miller J. M., Fabian A. C., 2009, MNRAS, 395, L52
Reis R. C., Fabian A. C., Miller J. M., 2010, MNRAS, 402, 836
Russell D. M., Fender R. P., Gallo E., Kaiser C. R., 2007, MNRAS, 376, 1341
Russell D. M., Maitra D., Dunn R. J. H., Markoff S., 2010, MNRAS, 405, 1759
Rykoff E. S., Miller J. M., Steeghs D., Torres M. A. P., 2007, ApJ, 666, 1129
Sobolewska M. A., Papadakis I. E., Done C., Malzac J., 2011, MNRAS, 417, 280 (S11)
Takahashi T. et al., 2012, Proc. SPIE, Vol. 8443, Space Telescopes and Instrumentation 2012: Ultraviolet to Gamma Ray. SPIE, Bellingham, p. 84431Z
Torii S. et al., 2011, PASJ, 63, 771
Uttley P., Wilkinson T., Cassatella P., Wilms J., Pottschmidt K., Hanke M., Böck M., 2011, MNRAS, 414, L60
Veledina A., Vurm I., Poutanen J., 2011, MNRAS, 414, 3330
Veledina A., Poutanen J., Vurm I., 2012, MNRAS, 430, 4
Vurm I., Poutanen J., 2009, ApJ, 698, 293
Xie F.-G., Yuan F., 2012, MNRAS, 427, 1580
Yamada S., Makishima K., Done C., Noda H., Torii S., Sakurai S., 2013, preprint (arXiv:1304.1968)
Yu Z., Yuan F., Ho L. C., 2011, ApJ, 726, 87
Yuan F., Cui W., 2005, ApJ, 629, 408
Yuan F., Zdziarski A. A., 2004, MNRAS, 354, 953
Yuan F., Cui W., Narayan R., 2005, ApJ, 620, 905
Yuan F., Zdziarski A. A., Xue Y., Wu X.-B., 2007, ApJ, 659, 541
Yuan F., Yu Z., Ho L. C., 2009, ApJ, 703, 1034
Zdziarski A. A., Lubiński P., Gilfanov M., Revnivtsev M., 2003, MNRAS, 342, 355
Zdziarski A. A., Lubiński P., Sikora M., 2012, MNRAS, 423, 663

APPENDIX A: ACCRETION FLOW MODEL

The model consists of an outer blackbody disc (BB), truncated at some radius (R_t), with an inner hot flow of radius $R_{\rm hot}$, where $R_{\rm hot} = 20R_g$. The hot flow is taken to be radiatively inefficient, such that

$$L_{\rm hot} = L_{\rm BBdisc}(R < R_t)\left(\frac{\dot{m}}{\dot{m}_c}\right), \tag{A1}$$

where $\dot{m} = \dot{M}/\dot{M}_E$, $\dot{m}_c = 0.1$ and $L_{\rm BBdisc}(R < R_t)$ is the luminosity of a BB disc extending from the truncation radius down to the last stable orbit.

We scale the truncation radius with accretion rate, such that

$$\dot{R}_t = 20R_g\left(\frac{\dot{m}}{\dot{m}_c}\right)^{-1/2}. \tag{A2}$$

The optical depth (τ) of the Comptonizing region is fixed at 2 for $\dot{m} = \dot{m}_c$, and scales with $\dot{m}$ as

$$\tau = 2\left(\frac{\dot{m}}{\dot{m}_c}\right). \tag{A3}$$

The unabsorbed cyclo-synchrotron emission from the hot flow is calculated following Di Matteo, Celotti & Fabian (1997):

$$L_{\rm cyclo}(\nu) = 5.57\times10^{-29}\frac{n\nu I(x)V}{K_2(1/\theta_e)}, \tag{A4}$$

where $V = 2/3\pi R_{\rm hot}^3$ is the volume of the Comptonizing hot flow, n is the number density of electrons calculated from the optical depth, $\theta = kT/m_ec^2$ is the dimensionless electron temperature, $K_2(1/\theta)$ is the modified Bessel function, $x = 2\nu/3\nu_B\theta^2$, $\nu_B = eB/2\pi m_ec$ is the Larmor frequency and the function $I(x)$ is given by

$$I(x) = \frac{4.050}{x^{1/6}}\left(1+\frac{0.40}{x^{1/4}}+\frac{0.532}{x^{1/2}}\right)\exp(-1.8899x^{1/3}). \tag{A5}$$

The magnetic field (B) of the hot flow is calculated from the density by assuming the ions are at the virial temperature and the magnetic field is 10 per cent of the gas pressure, giving

$$B = \sqrt{0.1nm_pc^2\frac{8\pi}{r_{\rm hot}}}, \tag{A6}$$

where $r_{\rm hot} = R_{\rm hot}/R_g$. The cyclo-synchrotron self-absorption frequency is given by

$$\nu_{\rm csa} = \frac{3}{2}\nu_B\theta^2x_m, \tag{A7}$$

where x_m is found by solving for x when the cyclo-synchrotron and BB emission are set equal:

$$L_{\rm cyclo}(\nu_{\rm csa}) = 8\pi^2m_e\nu_{\rm csa}^2\theta_eR_{\rm hot}^2. \tag{A8}$$

Below the self-absorption frequency the absorbed emission is calculated as

$$L(\nu < \nu_{\rm csa}) = \left(\frac{\nu}{\nu_{\rm csa}}\right)^{5/2}L(\nu_{\rm csa}). \tag{A9}$$

Thermal Comptonization is modelled using EQPAIR (Coppi 1999), with seed photons from both the disc and cyclo-synchrotron emission, where the fraction of disc photons from a given radius (R) intercepted by the hot flow is given by

$$\frac{L_{\rm seed,disc}}{L_{\rm disc}} = \left(\frac{R_{\rm hot}}{R}\right)\frac{\arcsin(R_{\rm hot}/R)}{\pi}, \tag{A10}$$

and we calculate the mean seed photon temperature

$$kT_{\rm seed} = \frac{k(L_{\rm seed,disc}T_{\rm disc}+L_{\rm cyclo}T_{\rm cyclo})}{L_{\rm seed,disc}+L_{\rm cyclo}}. \tag{A11}$$

The electron temperature, a parameter in both the cyclo-synchrotron equations and EQPAIR, is calculated self-consistently.

A1 Jet model

We construct a conical jet, where opening angle ($\phi = 0.1$) relates jet radius ($R_{\rm j}$) to distance along the jet (z):

$$R_{\rm j}(z) = \phi z. \tag{A12}$$

We assume a fraction of the accreting material ($f_{\rm j}$) is diverted up the jet. The energy density in relativistic particles at the jet base is set to be some fraction ($f_{\rm rel} = 0.1$) of the magnetic energy density:

$$m_e c^2 \int_{\gamma_{\rm min}}^{\gamma_{\rm max}} \gamma n(\gamma) {\rm d}\gamma = U_{\rm rel,0} = f_{\rm rel} U_{B,0}. \tag{A13}$$

We conserve magnetic energy and particle number along the jet such that

$$B(z) = B_0 \left(\frac{z}{z_0}\right)^{-1}, \tag{A14}$$

$$K(z) = K_0 \left(\frac{z}{z_0}\right)^{-2}, \tag{A15}$$

and allow B_0 and K_0 to scale with accretion rate as

$$B_0 = B_0(\dot{m}_c) \left(\frac{\dot{m}}{\dot{m}_c}\right)^{1/2}, \tag{A16}$$

$$K_0 = K_0(\dot{m}_c) \left(\frac{\dot{m}}{\dot{m}_c}\right), \tag{A17}$$

where $\dot{m}_c = 0.1$, and $B_0(\dot{m}_c)$, $K_0(\dot{m}_c)$ and z_0 are fixed by requiring the radio luminosity and the optically thick–optically thin synchrotron break match observations of GX 339−4 (Gandhi et al. 2011).

We assume electrons in the jet are continually accelerated into a power-law distribution of the form:

$$n(\gamma) = K \gamma^{-p}, \tag{A18}$$

where $p = 2.4$, for electron Lorentz factors ranging from $\gamma = 1.0$ to 1×10^5.

We split the jet into conical sections and calculate the synchrotron emission from electrons in each section:

$$L_s(\nu) = \frac{\sigma_T c}{8\pi \nu_B} U_B \gamma n(\gamma) V \delta^3, \tag{A19}$$

where V is the volume of the conic section, $\delta = 1/(\Gamma - \cos\psi\sqrt{\Gamma^2 - 1})$ is the boosting factor of the jet, ψ is the angle of the jet with respect to the observer and the electron Lorentz factor and synchrotron photon frequency are related by $\gamma = \sqrt{3\nu/4\nu_B}$.

The synchrotron self-absorption frequency ($\nu_{\rm ssa}$) in each section is given by (Ghisellini et al. 1985)

$$\nu_{\rm ssa} = \left(4.62 \times 10^{14} K B^{2.5} \frac{R_{\rm j}}{0.7}\right)^{2/7}. \tag{A20}$$

The frequency of the observed radiation is boosted by a factor of $\nu_{\rm obs} = \nu\delta$. We neglect synchrotron self-Comptonization.

This paper has been typeset from a TEX/LATEX file prepared by the author.